AIP The Journal of Chemical Physics

Proton-transport catalysis and proton-abstraction reactions: An ab initio dynamical study of X+HOC + and XH + + CO (X=Ne, Ar, and Kr)

Michael A. Collins, Simon Petrie, Andrew J. Chalk, and Leo Radom

Citation: The Journal of Chemical Physics **112**, 6625 (2000); doi: 10.1063/1.481235
View online: http://dx.doi.org/10.1063/1.481235
View Table of Contents: http://scitation.aip.org/content/aip/journal/jcp/112/15?ver=pdfcov
Published by the AIP Publishing

Proton-transport catalysis and proton-abstraction reactions: An *ab initio* dynamical study of $X+HOC^+$ and XH^++CO ($X=Ne$, Ar, and Kr)

Michael A. Collins,[a] Simon Petrie, Andrew J. Chalk, and Leo Radom
Research School of Chemistry, Australian National University, Canberra, ACT, 0200, Australia

(Received 29 December 1999; accepted 19 January 2000)

Ab initio potential energy surfaces have been constructed and used to carry out classical simulations of the reactions of X with HOC^+ and of XH^+ with CO ($X=Ne$, Ar, and Kr). The competition between rearrangement, $X+HOC^+\rightarrow OCH^++X$, and abstraction, $X+HOC^+\rightarrow XH^++CO$, has been examined, and found to favor abstraction in the cases where both processes are energetically allowed. The reaction of XH^+ with CO is found to produce highly vibrationally excited $[CHO]^+$ products. © *2000 American Institute of Physics.* [S0021-9606(00)01414-8]

I. INTRODUCTION

It is well established that the isoformyl cation (HOC^+) is much less stable than its isomer, the formyl cation (HCO^+), the energy difference being approximately 160 $kJ\,mol^{-1}$.[1–11] However, because there is a substantial barrier of about 150 $kJ\,mol^{-1}$ separating the two forms,[1–7,11] both isomers can be separately observed as stable species in the gas phase.[8–10,12–14] For example, the microwave spectra of both HOC^+ and HCO^+ have been recorded.[12,13] In addition, both HOC^+ and HCO^+ are firmly established interstellar species.[15–17]

The barrier for the rearrangement of HOC^+ to HCO^+ has been found to be substantially reduced, or in some cases even eliminated, as the result of interaction with an appropriate neutral molecule (X).[1,10,14,18,11] This is an example of what Bohme has described as catalyzed proton transport,[19] or what may be referred to more generally as ion-transport catalysis.[20]

The reason for the barrier lowering is straightforward. Complexation of X with HOC^+ weakens the $H\cdots O$ bond, thus facilitating the rearrangement:

$$X+HOC^+\rightarrow[XH\cdots OC]^+\rightarrow[OC\cdots HX]^+\rightarrow OCH^++X. \tag{1.1}$$

Equivalently, we note that the proton is more weakly bound in the transition structure for rearrangement than in the reactant or product ions and is therefore able to interact more effectively with X. A recent systematic theoretical study of the $[XCHO]^+$ system,[18] found that when X has a proton affinity less than that of CO at either O or C (e.g., $X=He$, Ne, and Ar), the barrier to rearrangement is reduced but not eliminated. In cases where X has a proton affinity lying between that of CO at O and C (e.g., $X=HF$ and N_2), the barrier disappears. Finally, for molecules X with a proton affinity greater than that of CO at O or C (e.g., $X=H_2O$ and NH_3), the barrier for rearrangement again disappears, but in such cases an alternative reaction, hydrogen abstraction, is energetically preferred:

$$X+HOC^+\rightarrow XH^++CO. \tag{1.2}$$

Although the calculations of the *energies* of reactions (1.1) and (1.2) provide valuable information, it is of interest to go further and investigate the *dynamics* of these reactions. As a first step in this direction, we examine in this paper the reactions of HOC^+ with the rare gas atoms $X=Ne$, Ar, and Kr, first to establish the feasibility of constructing complete potential energy surfaces (PES) for such systems, and second to study the dynamical competition between rearrangement and abstraction. We are currently investigating the reactions of HOC^+ with other prototypical small molecules.

We begin by expanding the previous theoretical investigations of the interactions of the $[CHO]^+$ isomers with Ne and Ar to the case of Kr. We then present complete potential energy surfaces for all three $[XCHO]^+$ systems and use these to estimate (with classical dynamics) the cross sections for reactions (1.1) and (1.2). Our investigation also yields results for the hitherto unstudied, but experimentally accessible, reactions of XH^+ ($X=Ne$, Ar, and Kr) with CO:

$$XH^++CO\rightarrow X+[CHO]^+. \tag{1.3}$$

Cross sections for proton transfer to CO are presented, and the branching ratio of the isomeric product ions, HCO^+/HOC^+, is evaluated and discussed in the context of the energies with which they are produced. We note that the reaction of HOC^+ with Kr has been the subject of a previous experimental study[10] and found to have a very low reaction rate, despite the very small difference in the proton affinities of Kr($PA=424.6$ $kJ\,mol^{-1}$)[21] and of CO at O ($PA=426.3$ $kJ\,mol^{-1}$).[10,21]

The paper is set out as follows. Section II presents a brief comparison of the accuracy of various levels of *ab initio* theory for these systems, largely for the purpose of identifying a suitable level to investigate $[KrCHO]^+$. This section also briefly describes the interpolation method used to construct the PES for all three cases. The results presented in Sec. III include a qualitative description of the PES in terms of the energy profiles on the relevant reaction paths and the classical simulations of both $X+HOC^+$ and XH^++CO collisions, with predictions for the reaction cross sections. The paper finishes with some concluding remarks in Sec. IV.

[a]Electronic mail: collins@rsc.anu.edu.au

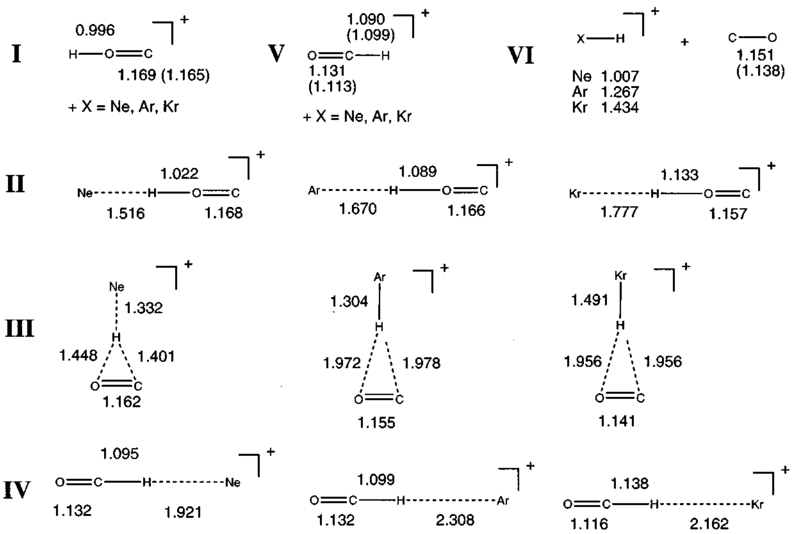

FIG. 1. Schematic representation of stationary points on the potential energy surfaces for $[NeCHO]^+$, $[ArCHO]^+$, and $[KrCHO]^+$. The geometries for the neon and argon systems have been optimized at the MP2/6-31G(d,p) level of theory, and for the krypton system at the B3-LYP/6-31G(d,p) level of theory. The bond lengths in parentheses refer to B3-LYP/6-31G(d,p) values.

II. POTENTIAL ENERGY SURFACES

A. Levels of *ab initio* theory

The *ab initio* calculations reported herein have been carried out using the GAUSSIAN 94 and GAUSSIAN 98 suites of programs[22,23] and have employed spin-restricted (R) formalisms.

A previous systematic *ab initio* study of $[NeCHO]^+$, $[ArCHO]^+$, and related systems[18] showed that the MP2/6-31G** level of theory satisfactorily determines the geometries of the various stationary points on the PES to reasonable accuracy. These optimized geometries are displayed in Fig. 1. However, accurate evaluation of the energies of these stationary points requires higher levels of theory, and a modification of the composite G2 method, termed G2**, was selected.[18] Although the energies of stationary points for $[NeCHO]^+$ and $[ArCHO]^+$ at the MP2/6-31G** level of theory can differ from the values given by G2** calculations by tens of kJ mol^{-1} (see Table I), the energy range of these features on the PES is sufficiently large (nearly 400 kJ mol^{-1} for $[NeCHO]^+$ and about 220 kJ mol^{-1} for $[ArCHO]^+$) that the MP2/6-31G** surfaces are relatively good approximations to the exact PES. Since construction of each PES requires evaluation of the energy gradients and second derivatives at several hundred configurations, we have adopted MP2/6-31G** as a suitable compromise level for the computations for $[NeCHO]^+$ and $[ArCHO]^+$.

For the $[KrCHO]^+$ system, a comparison of the performance of several different levels of *ab initio* theory was undertaken in order to identify a method that would be sufficiently accurate yet computationally feasible for the subsequent reaction dynamics investigation. Reaction (1.2) is endoergic without any intermediate barrier, while reaction (1.1) involves an intermediate transition structure whose energy lies close to that of the reactants. The height of the barrier in reaction (1.1) and the relative energy of the reactants and products in reaction (1.2) appear to be suitable parameters by which to judge the accuracy of the various levels of *ab initio* theory.

A reference value for the endothermicity of reaction

TABLE I. Relative energies (kJ mol^{-1}) of structures in Fig. 1, evaluated using MP2/6-31G(d,p) for $[NeCHO]^+$ and $[ArCHO]^+$ and using B3-LYP/6-31G(d,p) for $[KrCHO]^+$, are compared with results obtained using G2** theory and with experimental data.

	Relative energies								
	$NeCOH^+$			$ArCOH^+$			$KrCOH^+$		
Structure	MP2[a]	G2**[b]	Expt[c]	MP2[a]	G2**[b]	Expt[c]	B3-LYP[d]	G2(QCI)**[e]	Expt[c]
I	0	0	0	0	0	0	0	0	0
II	−27	−15		−35	−49		−73	−61	
III	113	131		43	33		1	−8	
IV	−195	−163		−191	−174		−180	−177	
V	−180	−158	−167	−180	−158	−167	−145	−154	−167
VI	209	228	226	63	52.3	56	24	18	2

[a]MP2/6-31G** with a zero-point energy correction scaled by 0.937 (Ref. 18).
[b]Modified G2 theory (Ref. 18).
[c]From differences in proton affinities at 298 K (Refs. 9 and 10).
[d]B3-LYP/6-31G** in which the basis includes pure d functions, and including an unscaled zero-point energy correction.
[e]G2(QCI)** is a modified form of G2 theory in which the additivity approximations are eliminated.

TABLE II. Relative energies (kJ mol^{-1}) of stationary points and dissociated products on the [KrCHO]$^+$ potential energy surface.

Method	Kr+HOC$^+$	Kr···HOC$^+$	KrH$^+$···(CO)TS	OCH···Kr$^+$	OCH$^+$+Kr	KrH$^+$+CO
HF6-31G**	0	−34.0	+67.5	−142.0	−123.5	+69.8
Hybrid MP2[a]	0	−40.0	+26.2	−209.7	−188.2	+49.7
MP2(fu)/6-31G**	0	−58.6	+8.7	−213.3	−188.7	+24.9
B3-LYP/6-31G**[b]	0	−70.6	+6.8	−187.9	−153.2	+31.4
HF/6-311G**	0	−30.0	+53.6	−148.9	−137.3	+53.2
B3-LYP/6-311G**	0	−65.6	+0.5	−190.0	−164.0	+17.4
MP2(fc)/6-311G**[c]	0	−59.3	−6.5	−215.7	−198.1	+4.1
MP2(fc)/6-311G**[d]	0	−59.4	−5.6	−215.8	−198.1	+5.4
MP2(fu)/6-311G**	0	−59.4	−6.3	−216.6	−198.5	+4.8
QCISD(fc)/6-31G*	0	−44.9	+30.7	−186.4	−164.5	+43.5
G2(QCI)**[e]-ZPE[f]	0	−64.1	−5.7	−189.4	−164.8	+21.9
Expt[g]-ZPE[f]	0				−177.3	+6.0
G2(QCI)**[e]	0	−60.7	−8.2	−177.2	−154.2	+17.6
Expt[g]	0				−166.7	+1.7

[a]MP2 calculations with a 6-31G(d,p) basis for C, H, and O and a LanL2DZ basis (Ref. 25) for krypton with effective core potential (ECP)—Ref. 26.
[b]Using a basis which includes pure d functions (Ref. 25).
[c]MP2(fc)/6-311G** with the 3d orbitals frozen.
[d]MP2(fc)/6-311G** with the 3d orbitals correlated.
[e]QCISD(T)/6-311+G(3df,2p) energies evaluated at geometries optimised at the MP2(fu)/6-31G** level, with the ZPE correction described in footnote f.
[f]The zero-point energy (ZPE) was evaluated from HF/6-31G(d,p) harmonic vibrational frequencies and scaled by 0.8929.
[g]From Ref. 21.

(1.2) for the [KrCHO]$^+$ system may be obtained from the difference ΔPA(CO,Kr) between the experimental values of the proton affinity of CO at O and the proton affinity of Kr.[21] This leads to an endothermicity of 1.7 kJ mol^{-1}. However, it should be noted that there are some grounds for suspecting that the present literature experimental values[21] may underestimate the true ΔPA(CO,Kr). First, in the sole experimental study of the reaction of HOC$^+$ with Kr, only a very slow proton-transfer reaction and no apparent conversion to HCO$^+$ were observed, with an overall reaction rate coefficient of 4.0×10^{-10} cm^3 molecule^{-1} s^1 at 300 K.[10] This rate coefficient is about an order of magnitude lower than would be expected if the reaction lacked any activation barrier other than the reaction endothermicity (as is usually assumed for gas-phase proton-transfer reactions), suggesting that the true ΔPA(CO,Kr) may be greater than the accepted value. Second, the highest level of theory that we employ, G2(QCI)** (see Table II), gives a significantly larger ΔPA(CO,Kr) of 17.6 kJ mol^{-1} (which is almost identical to the B3-LYP/6-311G** value). Since the G2 family of computational techniques has been found generally to be quite reliable in determining proton affinities,[24] this is considered good evidence for a ΔPA(CO,Kr) larger than the current experimental value.

From Table II we see that Hartree–Fock calculations and quadratic configuration interaction calculations, including single and double substitutions (QCISD) using a 6-31G* basis set, give large relative energies for KrH$^+$+CO [i.e., large ΔPA(CO,Kr) values]. Second-order Møller–Plesset perturbation theory using a 6-31G** basis set with correlation of all electrons is (perhaps fortuitously) in close agreement with the G2(QCI)** calculation for KrH$^+$+CO. Out of a number of other levels of *ab initio* theory examined for [KrCHO]$^+$, the best agreement with experiment is found for ''standard'' full or frozen-core MP2/6-311G** calculations, with very little difference in relative energies seen when either the Kr 3d orbitals, or all ''core'' orbitals, are included in the correlation space. Unfortunately, MP2/6-311G** is much too demanding of CPU time for our present purposes. Of the remaining methods, B3-LYP/6-311G** performed best, as measured by overall agreement with experiment, but it is also computationally too intensive to employ here.

The B3-LYP/6-31G** level of theory was considered to provide a reasonable compromise between accuracy and expense, and has been used for surface construction in the present study. It has a somewhat larger discrepancy with the experimental ΔPA(CO,Kr) value than some of the other procedures but it is computationally much less demanding. It also has the virtue that it gives a substantially lower barrier to isomerization than do the other 6-31G** methods, and this was judged useful in modeling a system thought likely to lack a significant isomerization barrier. The B3-LYP/6-31G** energies of the relevant stationary points for the [KrCHO]$^+$ system, corresponding to the optimized geometries of Fig. 1, are included for comparison in Table I.

B. Form of the potential energy surface (PES)

The PES is given by an interpolation of Taylor expansions centered at data points scattered throughout the configuration space of the system[27–32] The surface can be constructed using all the interatomic distances, $\mathbf{R}=\{R_1,R_2,..,R_6\}$ as coordinates. In practice, we use inverse distances, $\mathbf{Z}$, rather than bond lengths, where $Z_k=1/R_k$. The potential energy at a configuration, $\mathbf{Z}$, in the vicinity of a data point, $\mathbf{Z}(i)$, can be expanded as a Taylor series to second order, T_i:

$$T_i(\mathbf{Z})=V[\mathbf{Z}(i)]+\sum_{k=1}^{6}[Z_k-Z_k(i)]\frac{\partial V}{\partial Z_k}\bigg|_{\mathbf{Z}=\mathbf{Z}(i)}+\frac{1}{2!}\sum_{k=1}^{6}\sum_{j=1}^{6}[Z_k-Z_k(i)]\times[Z_j-Z_j(i)]\frac{\partial^2 V}{\partial Z_k\partial Z_j}\bigg|_{\mathbf{Z}=\mathbf{Z}(i)}+\dots. \quad (2.1)$$

$V[\mathbf{Z}(i)]$ is the total electronic energy at the configuration $\mathbf{Z}(i)$. The Cartesian first and second derivatives of the energy are also evaluated at this configuration and transformed into derivatives with respect to inverse distances at $\mathbf{Z}(i)$.

If the required energies and derivatives have been evaluated at each of N_d molecular configurations, a modified Shepard interpolation[33,34] gives the potential energy at any configuration $\mathbf{Z}$ as a weighted average of the Taylor series about all N_d data points,[31]

$$V(\mathbf{Z})=\sum_{i=1}^{N_d} w_i(\mathbf{Z})T_i(\mathbf{Z}). \quad (2.2)$$

The weight function, w_i, which gives the contribution of the ith Taylor expansion to the potential energy at the configuration $\mathbf{Z}$, has been discussed in detail elsewhere.[32,35] In qualitative terms, we would like the Taylor series, T_i, which is most accurate at $\mathbf{Z}$ to have the highest weight in Eq. (2.2). However, since we do not know *a priori* which Taylor series is most accurate, a procedure for determining the relative weight for each data point must be established. First, the weights are normalized (sum to unity) by setting

$$w_i(\mathbf{Z})=\frac{\nu_i(\mathbf{Z})}{\sum_{k=1}^{N_d}\nu_k(\mathbf{Z})}. \quad (2.3)$$

One can show that Eq. (2.2) is an interpolation of the energy and of the first and second derivatives at the data points, and that Eq. (2.2) becomes exact in the limit of infinite data density, for appropriate choices of the weight functions.

To bias the weight function toward the Taylor expansions most likely to be accurate, the unnormalized weight function, ν_i, is given by

$$\nu_i(\mathbf{Z})=\left\{\left[\sum_{k=1}^{6}\left(\frac{Z_k-Z_k(i)}{d_k(i)}\right)^2\right]^q+\left[\sum_{k=1}^{6}\left(\frac{Z_k-Z_k(i)}{d_k(i)}\right)^2\right]^p\right\}^{-1}, \quad (2.4)$$

where $q=2$ and $p=12$.[32] The quantities $\{d_k(i),k=1,...,6\}$ define a confidence volume about the ith data point. If $\sum_{k=1}^{6}(Z_k-Z_k(i))^2/d_k(i)^2\ll 1$, then the weight of the ith data point at $\mathbf{Z}$ varies only with the low power q, while if $\sum_{k=1}^{6}(Z_k-Z_k(i))^2/d_k(i)^2\gg 1$, the weight of the ith data point is rapidly damped by the high power, p. The confidence lengths, $\{d_k(i)\}$, are determined by a Bayesian analysis of the inaccuracy of the ith Taylor expansion at M configurations close to $\mathbf{Z}(i)$:[32]

$$d_n(i)^{-6}=\frac{1}{M}\sum_{k=1}^{M}\frac{\left\{\left[\frac{\partial V[\mathbf{Z}(k)]}{\partial Z_n}-\frac{\partial T_i[\mathbf{Z}(k)]}{\partial Z_n}\right][Z_n(k)-Z_n(i)]\right\}^2}{E_{\mathrm{tol}}^2\|\mathbf{Z}(k)-\mathbf{Z}(i)\|^6}. \quad (2.5)$$

The $\{\mathbf{Z}(k)\}$ are taken to be the nearest M neighboring data points of the remaining (N_d-1) points in the data set. The error tolerance, E_{tol}, defines the accuracy required for $\mathbf{Z}$ to lie within the confidence volume of $\mathbf{Z}(i)$. As discussed elsewhere, the accuracy of Eq. (2.2) is relatively insensitive to the values of M and E_{tol}. We have taken $M=36$ and $E_{\mathrm{tol}}=0.26\,\mathrm{kJ\,mol^{-1}}$ (0.1 mhartree).

C. Iterative development of the PES

The location of the data points in Eq. (2.2) has been determined using the iterative methods developed previously.[27,28,31] An initial investigation of each potential energy surface was carried out by performing geometry optimizations at the appropriate level with the GAUSSIAN 94 or GAUSSIAN 98 programs, with initial geometries corresponding to the asymptotic reactants and products of reactions (1.1)–(1.3). The saddle point for isomerization, structure II of Fig. 1, was also located for each system, and geometry optimizations were initiated there to determine the paths leading to the minima, corresponding to $X\cdots HOC^+$ and $OCH\cdots X^+$ structures. For each system, approximately 100 geometries were selected from those encountered during these minimizations to form an initial data set which roughly describes the principal minimum energy paths for reactions (1.1)–(1.3).

The potential of Eq. (2.2) is then well defined in the vicinity of the reaction paths. Classical trajectories are evaluated, with initial conditions appropriate to the reaction(s) of interest, to explore the relevant region of configuration space. Molecular configurations encountered during these trajectories are recorded. One or more of these configurations is then chosen to be a new data point. The *ab initio* energy, gradient, and second derivatives are evaluated at that point and the data point is added to the set, generating a new version of the PES. This process of simulating the reaction(s), choosing an additional configuration, performing the *ab initio* calculations at that point and adding the new data point to the set is repeated again and again until the PES is held to be ''converged.'' Convergence is established by performing large-scale classical simulations of the reaction(s) of interest periodically during the ''growth'' of the data set. When the observable properties of interest, e.g., a rate coefficient or a cross section, do not change with increasing data set size, the PES is taken to be converged.

The methods for choosing a new data point from the ''trajectory configurations'' have been discussed in detail elsewhere.[31] The ''variance sampling'' method places data points at configurations where the uncertainty in Eq. (2.2) is highest, i.e., we evaluate δ for each of the recorded trajectory configurations:

$$\delta^2=\sum_{i=1}^{N_d} w_i(\mathbf{Z})[T_i(\mathbf{Z})-V(\mathbf{Z})]^2. \quad (2.6)$$

The configuration with largest δ is added to the data set. The alternative $h[\mathbf{Z}]$ or ''h weight'' method[27,28,31] attempts to place data in regions where the trajectories often visit, but where few data points are already present. Here we have used the ''variance sampling'' and ''h weight'' methods alternately for each additional data point.

D. Computational details

All classical trajectories performed, both during the iterative construction of the PES and to evaluate the scattering dynamics, were carried out using the standard methods previously detailed.[28–31] A step size of 1×10^{-17} s was used in the velocity-Verlet integration algorithm[36] for the Ne and Ar systems, and 2×10^{-17} s for the Kr case. The reactants were initially separated by 7.41 Å($14\,a_0$) for trajectories involving Ne, and 9.0 Å($17\,a_0$) for Ar and Kr. Trajectories were terminated when any bond length exceeded the initial separation of the reactants while the molecular fragments were separating (rather than coming closer together). The maximum impact parameter was 2.6 Å($5\,a_0$) during the construction of the PES.

All reactant molecules were given an initial microcanonical distribution of vibrational energy, for a total energy roughly approximating the value of the zero-point energy: 34.9 kJ mol^{-1} for HOC$^+$, 12.6 kJ mol^{-1} for CO, 16.8 kJ mol^{-1} for NeH$^+$, 23.6 kJ mol^{-1} for ArH$^+$, and 14.5 kJ, mol^{-1} for KrH$^+$. Random initial velocities and configurations for the atoms in each fragment were evaluated using the efficient microcanonical sampling method of Schranz, Nordholm, and Nyman.[37] The molecular fragments were initially randomly oriented and given zero rotational angular momentum, using a program also due to Schranz. The initial relative translational energy of the reactants was set to 13.13 kJ mol^{-1} (5 mhartree) for all trajectories used in the construction of all PES.

For [NeCHO]$^+$, all trajectories performed for the construction of the PES were initiated with NeH$^+$+CO as reactants. The iterative procedure was repeated until the data set contained 728 points.

For [ArCHO]$^+$, 66 data points were selected from approximate minimum energy paths for reactions (1.1)–(1.3). Using trajectories initiated from both ArH$^+$+CO and Ar+HOC$^+$, points were iteratively added to the data set until it contained 509 points. At this stage, the data set contained very little data for well-separated reactants. To improve the accuracy of the PES in these regions, further iterations of the construction algorithm were performed with trajectories from both ArH$^+$+CO and Ar+HOC$^+$, performed over very short times to give samples of configurations biased to the asymptotic regions, until the data set contained 570 points. Finally, the intrinsic reaction paths for all reactions were evaluated by steepest descent in mass-weighted Cartesian coordinates on the interpolated PES. It was found that several minor ''bumps and dips'' were apparent on these paths for [ArCHO]$^+$, so for aesthetic purposes further data points were added near these imperfections until the data set for [ArCHO]$^+$ contained 590 points in total.

For [KrCHO]$^+$, 149 data points were selected from approximate minimum energy paths for reactions (1.1)–(1.3). Using trajectories initiated from both KrH$^+$+CO and Kr+HOC$^+$, points were iteratively added to the data set until it contained 1180 points. Again, further data points were added to the set in the asymptotic regions, and where steepest descent paths showed minor anomalous features. In practice, double minima were discovered in the hydrogen-bonding region, corresponding to [OCH···Kr]$^+$- and [OC···HKr]$^+$-type complexes. These minima appear to be of minor significance to the dynamics, since the barriers separating them are very small relative to the total energy available in these reactions. Nevertheless, additional data points were added in the vicinity of these minima to ensure that they were accurately described. The final data set then contained 1233 points. It should be noted that some difficulty in ''growing'' this PES resulted from the occasional tendency of the B3-LYP calculation to converge to an excited electronic state. Before this problem was recognized, such data points produced unphysical features in the PES and very possibly distorted the allocation of locations for subsequent data points. The data points for excited states were eliminated from the data set, and subsequent calculations using the PES ignore all data points whose energy is more than about 90 kJ mol^{-1} above that of KrH$^+$+CO. However, much of the data set was constructed before the most recent interpolation methodology, described previously, had become available.[32] The older methods are naturally less accurate and hence less efficient. This partly explains why a larger data set was required for [KrCHO]$^+$ to obtain an interpolation accuracy similar to that obtained for [NeCHO]$^+$ and [ArCHO]$^+$.

E. Accuracy of the PES

Some indication of the interpolation error remaining in the final PES can be gained from considering the average interpolation error in a sample of molecular configurations. A total of 1000, 900, and 722 molecular configurations were generated by random sampling of configurations encountered in classical trajectories for the [NeCHO]$^+$, [ArCHO]$^+$, and [KrCHO]$^+$ systems, respectively. The *ab initio* energy was evaluated at each configuration and compared with the value given by the interpolated PES. The final PES have average interpolation errors, in these samples, of 0.6, 0.5, and 1.1 kJ mol^{-1}, respectively. These average errors represent 0.1%, 0.2%, and 0.4%, respectively, of the energy ranges of these sampled configurations. In previous studies, interpolated PES with a comparably high level of accuracy have been sufficiently accurate to describe classical reaction rate coefficients.[38–41]

III. RESULTS AND DISCUSSION

A. Minimum energy paths

To provide a pictorial representation of the ''shape'' of these six-dimensional PESs, Figs. 2–4 present the energy profiles along the minimum energy paths for reactions (1.1)–(1.3). These paths were obtained from the interpolated PES by following the paths of steepest descent in mass-weighted Cartesian coordinates which lead from various local energy maxima and from the asymptotic configurations. The reac-

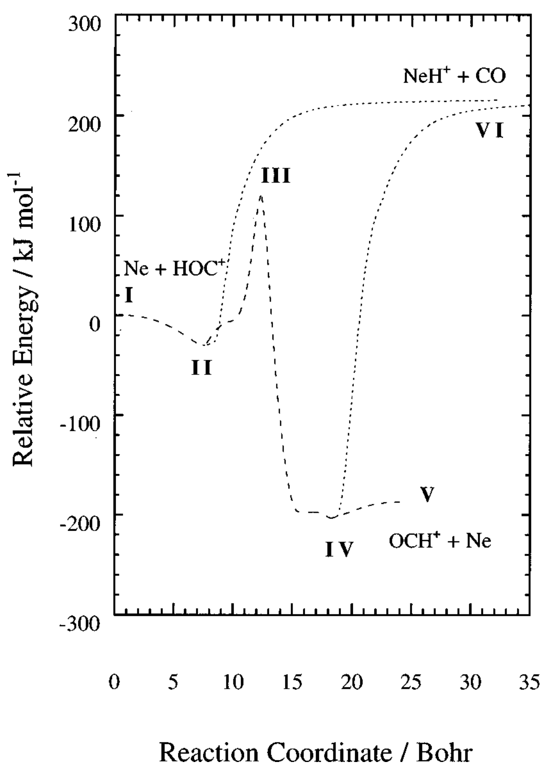

FIG. 2. The energy profile along minimum energy paths on the $[\mathrm{NeCHO}]^+$ surface is shown as a function of a reaction coordinate (see the text). The labeled stationary points are sketched in Fig. 1.

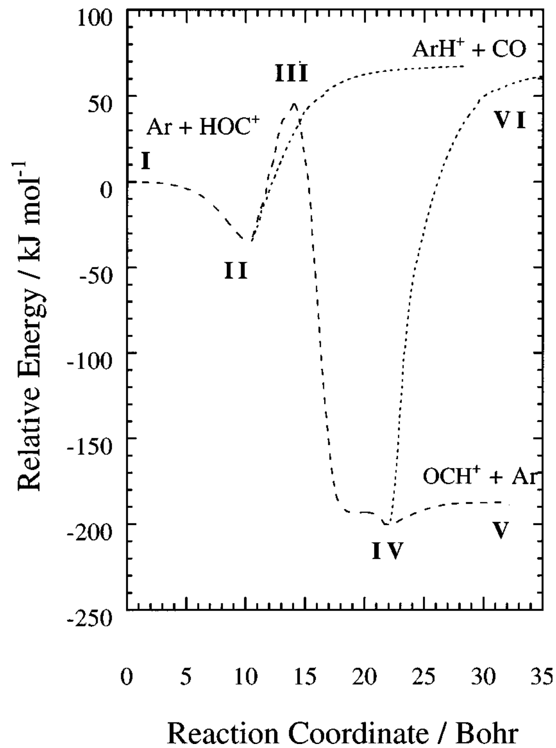

FIG. 3. The energy profile along minimum energy paths on the $[\mathrm{ArCHO}]^+$ surface is shown as a function of a reaction coordinate (see the text). The labeled stationary points are sketched in Fig. 1.

tion coordinate employed in Figs. 2–4 is a path length S, for which $dS=\|d\mathbf{R}\|$. The arbitrary origins and directions for each segment of the path have been adjusted for pictorial convenience. It is apparent from Figs. 2–4 that there are double minima in the hydrogen-bonding region, corresponding to $[\mathrm{OCH}\cdots\mathrm{X}]^+$ and $[\mathrm{OC}\cdots\mathrm{HX}]^+$-type complexes. The equilibrium geometries for the hydrogen-bonded structures are linear, but appear to be somewhat ''floppy.''

B. Isomerization versus abstraction in $\mathrm{X}+\mathrm{HOC}^+$ collisions

For $[\mathrm{NeCHO}]^+$, the barrier for isomerization of $\mathrm{Ne}+\mathrm{HOC}^+$ to $\mathrm{OCH}^+ + \mathrm{Ne}$ is not much less than that for isomerization of isolated HOC^+. In this case, there is no possibility of catalyzing the isomerization reaction at moderate energies, so we have therefore not investigated collisions of Ne with HOC^+. We discuss collisions of NeH^+ with CO below.

For $\mathrm{Ar}+\mathrm{HOC}^+$ as reactants, the barriers for isomerization to $\mathrm{OCH}^+ + \mathrm{Ar}$, and for abstraction to give $\mathrm{ArH}^+ + \mathrm{CO}$ are about 45.6 and 67.5 $\mathrm{kJ\,mol}^{-1}$, respectively (before correction for zero-point energy). The corresponding barriers after taking the zero-point energy into account are about 42.7 and 61.2 $\mathrm{kJ\,mol}^{-1}$. Table III presents the cross sections for the abstraction and isomerization reactions calculated from trajectory simulations for $\mathrm{Ar}+\mathrm{HOC}^+$ as reactants with a total energy of between 52.5 and 91.9 $\mathrm{kJ\,mol}^{-1}$ above the zero-point energy of the reactants. It should be noted immediately that the cross sections observed are very small. The statistical uncertainty from simulations of just 1000 trajectories is therefore sufficiently high that no attempt has been made to estimate the uncertainty in most cases. Clearly both isomerization and abstraction reactions are improbable, even at energies well above the classical thresholds. Significant cross sections are observed only for very highly excited HOC^+, where the abstraction reaction is about three times more likely than isomerization.

For $[\mathrm{KrCHO}]^+$, the barrier to isomerization is just 6.8 $\mathrm{kJ\,mol}^{-1}$ (before correction for zero-point energy), and just 1.1 $\mathrm{kJ\,mol}^{-1}$ after taking the zero-point energy into account. The energy required for the abstraction reaction is 31.4 $\mathrm{kJ\,mol}^{-1}$, or 24.5 $\mathrm{kJ\,mol}^{-1}$ after taking the zero-point energy into account. Table IV presents the cross sections for the abstraction and isomerization reactions, calculated from trajectory simulations of $\mathrm{Kr}+\mathrm{HOC}^+$ collisions for three different values of the relative translational energy, and approximately the zero-point vibrational energy. It is clear that, while the isomerization reaction dominates abstraction at low energy, the simpler abstraction process becomes more important at higher energy. It is important to note that the small cross sections for abstraction at the two lowest energies shown are artefacts of the classical approximation. The exact cross section is zero, since the *ground-state* KrH^+ plus CO products are energetically inaccessible: classical trajectories can (and do) produce KrH^+ and CO molecules with internal energy below the zero-point energy level.

At the lowest energy studied, the isomerization reaction catalyzed by Kr has a cross section of about 7.6 Å^2, which represents only about 8% of the Langevin ion–molecule capture cross section (calculated using the experimental polarizability of Kr[42]). Thus, while Kr does catalyze the isomeriza-

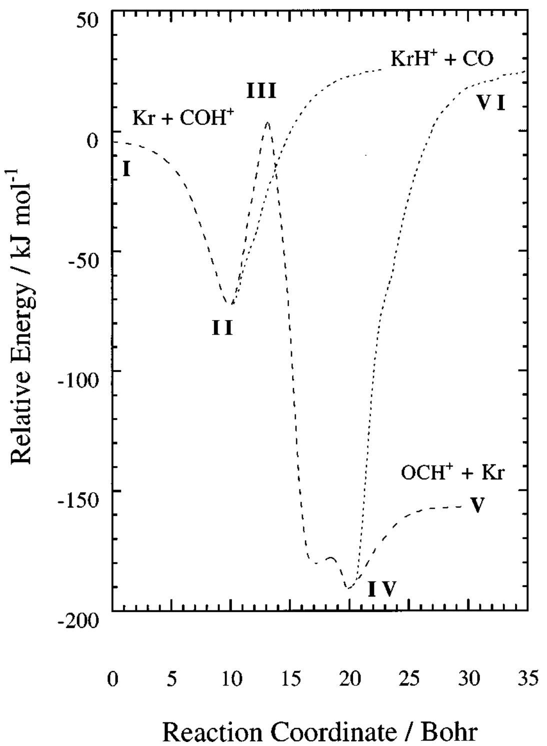

FIG. 4. The energy profile along minimum energy paths on the $[KrCHO]^+$ surface is shown as a function of a reaction coordinate (see the text). The labeled stationary points are sketched in Fig. 1.

tion of HOC$^+$ at low collision energies, the process is not particularly efficient. When the abstraction channel is open, this process proceeds at the expense of isomerization, as it does for Ar+HOC$^+$ collisions.

C. XH$^+$+CO reactions

1. Reaction cross sections

Table V presents a comparison of the reactive cross sections for XH$^+$+CO collisions, for X=Ne, Ar, and Kr. In these simulations, each reactant has approximately the zero-point vibrational energy, and the relative translational energy is 13.1 kJ mol^{-1} (5 mhartree). The final molecular configuration at the termination of each trajectory is counted as XH$^+$+CO if the X–H bond is short. If the X–H bond is long and the H–C bond is shorter than the H–O bond then the configuration is counted as X+HCO$^+$, while if the H–C bond is longer than the H–O bond then it is counted as X+HOC$^+$.

The results in Table V indicate that formation of HCO$^+$ is favored over formation of HOC$^+$ by a factor of about 2–3 in all cases. Note also that the total cross section for both abstraction reactions falls slightly in going from NeH$^+$ to ArH$^+$ to KrH$^+$. Since all three XH$^+$+CO collisions would be expected to have very similar Langevin capture cross sections,[43] this trend would appear to imply an increasing degree of steric hindrance in the sequence from Ne to Kr: reaction might be inhibited if the rare gas atom, rather than the hydrogen atom, impacts on the CO molecule. Evidence for such a steric effect can be obtained by examining the reaction probability as a function of impact parameter in the XH$^+$+CO collisions. Figure 5 presents the reaction probability as a function of impact parameter, evaluated for XH$^+$+CO collisions under the same conditions as mentioned earlier. Allowing for the large statistical errors, we can see that the reaction probability at small impact parameter is about 0.8 for both NeH$^+$ and ArH$^+$ colliders, though the probability of reaction falls to zero a little faster for ArH$^+$ than for NeH$^+$. Despite the statistical uncertainty apparent in Fig. 5, it is also clear that the probability of reaction for KrH$^+$+CO does not rise much above 0.6 at small impact parameter.

2. Energy distribution in the products

The cross sections of Table V result from an allocation of the product geometry in each trajectory as described previously. However, these allocations relate to a single ''snap shot'' of the molecular geometry at one instant. If the

TABLE III. Classical reaction cross sections (square angstroms) for products from Ar+HOC$^+$ collisions, calculated from 1000 trajectories, as a function of translational and vibrational energy (millihartrees).[a]

Translational energy	Vibrational energy[b]	Ar+HCO$^+$ cross section	ArH$^+$+CO cross section
5	ZPE+15	(0.17)	(0.34)[c]
5	ZPE+30	1.5±0.3	4.8±0.6
21	ZPE	(0.15)	(0.20)[c]
30	ZPE	(0.18)	(0.62)

[a]The statistical errors, where quoted, correspond to one standard deviation. Parentheses signify that the standard deviation cannot be accurately determined due to inadequate statistics for very small cross sections.
[b]ZPE denotes the zero-point energy, approximated as 13.3 mhartree (34.9 kJ mol^{-1}), see the text. 1 mhartree=2.625 kJ mol^{-1}.
[c]Ground-state products are energetically inaccessible, hence the correct quantum cross section is zero.

TABLE IV. Classical reaction cross sections (square angstroms) for products from Kr+HOC$^+$ collisions, calculated from 2000 trajectories in which the reactants have zero-point vibrational energy and selected values of the translational energy (millihartrees).[a]

Translational energy	Kr+HCO$^+$ cross section	KrH$^+$+CO cross section
3	7.6±0.8	1.9[b]
7.5	5.2±0.7	3.4[b]
15	2.3±0.4	5.8±0.7

[a]The statistical errors, where quoted, correspond to one standard deviation.
[b]Ground-state products are energetically inaccessible, hence the correct quantum cross section is zero.

TABLE V. Reaction cross sections (square angstroms) for XH$^+$+CO→X+HCO$^+$ and XH$^+$+CO→X+HOC$^+$ (X=Ne, Ar, and Kr, calculated from 2000 trajectories in which each reactant has approximately the zero-point vibrational energy, and the relative translational energy is 13.1 kJ mol^{-1} (5 mhartree).[a]

X	X+HCO$^+$ cross section	X+HOC$^+$ cross section
Ne	84.9±1.4	34.6±1.1
Ar	75.6±1.9	28.7±1.4
Kr	49.1±1.7	14.9±1.1

[a]The statistical errors correspond to one standard deviation.

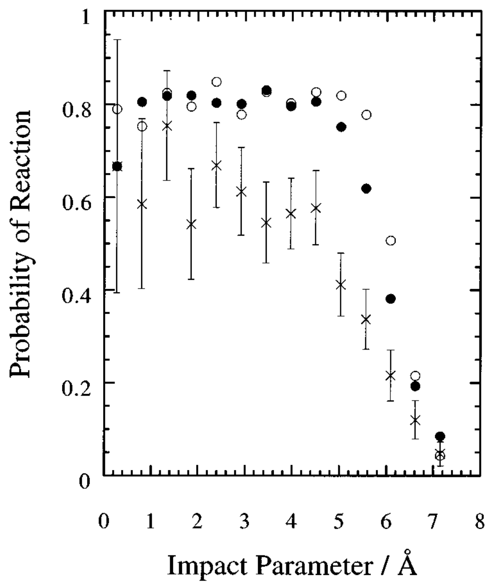

FIG. 5. The probability of reaction for $XH^+ + CO \rightarrow X + [CHO]^+$, for X=Ne (●), Ar (○), and Kr(×) is shown as a function of the impact parameter for the collision under the same reaction conditions as Table V. For clarity, error bars of two standard deviations are shown only on the data for krypton (they are very similar for the neon and argon data).

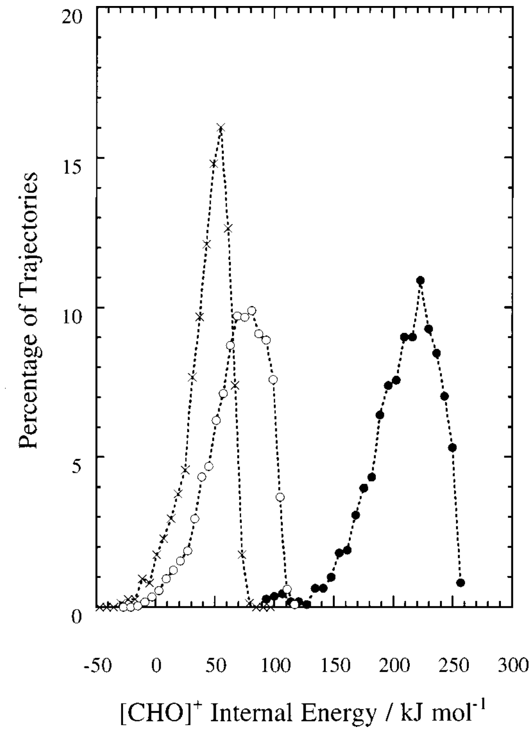

FIG. 6. The distribution of total internal energy in the $[CHO]^+$ products of the $XH^+ + CO$ reaction is shown for X=Ne (●), Ar(○), and Kr(×). The energy is shown relative to that of equilibrium HOC^+, and the distributions have been constructed from the trajectories used in Table V with a bin size of 6 kJ mol^{-1}.

$[CHO]^+$ fragment has sufficiently high energy, then the geometry of this fragment may oscillate between that of HOC^+ and HCO^+ as the X and $[CHO]^+$ moieties continue to separate. Figure 6 presents the distribution of internal energy in the $[CHO]^+$ fragment resulting from the three colliders, under the same conditions as mentioned previously. The variation in $[CHO]^+$ internal energy between the different systems can be seen to be substantial.

For $NeH^+ + CO \rightarrow Ne + [CHO]^+$, the reactant equilibrium geometry is about 215 kJ mol^{-1} above that of $Ne + HOC^+$. This energy is overwhelmingly directed into excitation of the $[CHO]^+$ product, which contains an average energy of 209 kJ mol^{-1} above equilibrium HOC^+. Over 96% of products have an internal energy of more than 147 kJ mol^{-1} above equilibrium HOC^+, which is the barrier height for the isomerization of isolated HOC^+, and *all* products observed have more than 34.9 kJ mol^{-1}, which is the approximate zero-point energy of HOC^+. Hence, metastable configurations corresponding to HOC^+ are energetically accessible for any product formed.

For $ArH^+ + CO \rightarrow Ar + [CHO]^+$, the reactant equilibrium geometry is about 68 kJ mol^{-1} above that of $Ar + HOC^+$. The $[CHO]^+$ product has an average energy of 69 kJ mol^{-1} above equilibrium HOC^+, and about 85% of the product $[CHO]^+$ ions have an energy above the zero-point energy of HOC^+. No products were observed to have an energy above the 147 kJ mol^{-1} barrier to isomerization, so that isomerization subsequent to the abstraction reaction is classically unlikely. Nevertheless, the $[CHO]^+$ product is generally sufficiently highly excited for tunnelling to occur between the HOC^+ and HOC^+ wells.

For $KrH^+ + CO \rightarrow Kr + [CHO]^+$, the reactant equilibrium geometry is only about 31 kJ mol^{-1} above that of $Kr + HOC^+$. The $[CHO]^+$ product has an average energy of only 43 kJ mol^{-1} above equilibrium HOC^+, but about 70% of the product $[CHO]^+$ molecules have an energy above the zero-point energy of HOC^+. Tunneling between the HOC^+ and HCO^+ wells is also feasible in this case for a majority of the product $[CHO]^+$ fragments, though presumably at a much slower rate than for the $[NeCHO]^+$ and $[ArCHO]^+$ systems.

3. Rotational angular momentum of the products

The classical simulations of all three $XH^+ + CO$ reactions have been carried out with zero rotational angular momentum in each of the reactant fragments. However, each system has considerable orbital angular momentum arising from the initial distribution of impact parameters. The average impact parameter for the reactive trajectories of Table V was found to be 7.8, 8.0, and 7.5 a_0 for the Ne, Ar, and Kr systems, respectively. These values correspond to average angular momenta of 115 $\hbar$, 139 $\hbar$, and 145 $\hbar$, respectively. Analysis of the $[CHO]^+$ products shows that the average rotational angular momenta are very similar for the three systems: 34 $\hbar$, 32 $\hbar$, and 27 $\hbar$, for the Ne, Ar, and Kr systems, respectively. Figure 7 illustrates the distribution of rotational angular momentum in the $[CHO]^+$ product for the $ArH^+ + CO$ reaction. Clearly the transfer of the proton to CO results in rotational excitation in the $[CHO]^+$ product, though most of the angular momentum must be in the form of orbital angular momentum of the separating fragments. Since we have seen that the $[CHO]^+$ product is highly rovibrationally excited, it is not possible to accurately separate

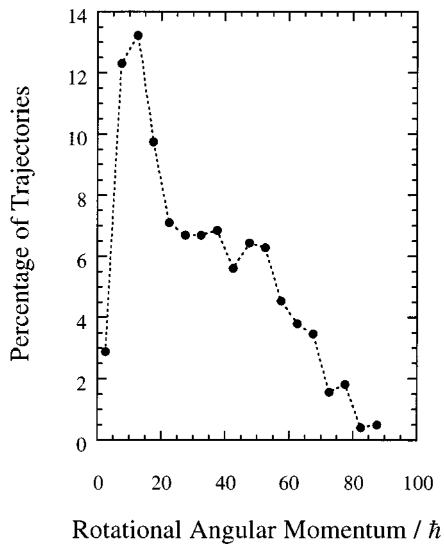

FIG. 7. The distribution of the magnitude of the rotational angular momentum of the $[CHO]^+$ products from the reaction $ArH^+ + CO$. The distribution was constructed from the trajectories used in Table V, with a bin size of 5 $\hbar$.

the energy of this fragment into rotation and vibration components. In a very crude approximation, we could model the HCO^+/HOC^+ system as a linear rotor with a moment of inertia of about 8 amu Å^2. The average angular momentum for this product in the Ne, Ar, and Kr systems would then correspond to rotational energies of 38, 34, and 24 kJ mol^{-1}, respectively. These are not especially high energies in comparison with the total rovibrational energy of the fragment relative to the most stable $[HCO]^+$ isomer. Hence, we might estimate that the greater part of the rovibrational energy in the $[CHO]^+$ product is in the form of vibrational energy.

IV. CONCLUDING REMARKS

We have considered the competition between the isomerization reaction (1.1) and the abstraction reaction (1.2) for collisions of Ar and Kr with HOC^+. For both systems, the isomerization product is energetically favored over the abstraction product, and the barrier to isomerization is lower than the energy required for abstraction. However, the isomerization process is generally not facile. For $Ar + HOC^+$ at energies above the barrier to isomerization but below that required for abstraction, the cross section for isomerization is extremely small. At higher energies where abstraction is allowed, this process dominates isomerization. For $Kr + HOC^+$, both the barrier to isomerization and the energy required for abstraction are lower than for $Ar + HOC^+$, and the resultant cross sections are significantly higher. Isomerization does proceed with a cross section of several square angstroms in the energy interval where isomerization is allowed but abstraction is not. However, the isomerization cross section falls well below that of abstraction when the latter process is energetically allowed. It is clear for the Ar and Kr colliders that abstraction competes directly with isomerization and dominates at energies for which both processes are possible.

It is reasonable to suggest that the dominance of abstraction over isomerization is due to entropic considerations. The transition state for isomerization is likely to be located near the saddle-point structure III (Fig. 1) in each case. The molecular rearrangement required to reach this region of configuration space is considerable, and the molecular vibrational frequencies at the saddle point are not low (a ''tight'' transition state).[44] In contrast, a variational treatment would be required to locate the transition state on the barrierless endoergic path to abstraction. It is likely that the transition state is quite late on this path, where the vibrational motion of XH^+ relative to CO resembles weakly hindered rotation. This very ''loose'' transition state[44] would favor a higher rate coefficient compared with that associated with the tight transition state for isomerization.

We have studied the reverse reaction (1.3) for all three rare gas colliders. The reactions are barrierless and show decreasing exothermicity in the sequence Ne, Ar, Kr. We have found that virtually all of the energy available from the reaction appears as internal energy in the $[CHO]^+$ fragment, while very little is released as relative kinetic energy of the separating fragments. The HCO^+ product is *initially* formed with a cross section 2.5–3.3 times that for HOC^+. However, these branching ratios for the HOC^+/OCH^+ products are *not* predictive. The ratio of HCO^+/HOC^+ products can be expected to change with time since the $[CHO]^+$ ions have sufficient energy to tunnel from one isomer to the other; the rate of such interconversion is expected to be much higher for the Ne system than for Ar or Kr.

The three systems examined in the present study provide a sequence in which the barrier to the isomerization reaction (1.1) is reduced, but never eliminated. We have found that isomerization is never facile, and is dominated by the abstraction reaction (1.2) when that process is energetically allowed. In future work, we will extend this sequence of reactions to cases where the barrier to isomerization is eliminated, and to cases where the abstraction reaction is also barrierless.

The data files and all software required to evaluate the PES for these and other systems are available via the Internet and anonymous ftp: (http://www.rsc.anu.edu.au/RSC/ChemResearch/Groups/DD-home.html and ftp://rsc.anu.edu.au/pub/collins/).

ACKNOWLEDGMENT

We gratefully acknowledge a generous allocation of computer time on the Fujitsu VPP-300 and SGI Power Challenge computers of the Australian National University Supercomputer Facility.

[1] R. H. Nobes and L. Radom, Chem. Phys. **60**, 1 (1981).
[2] J. E. Del Bene, M. J. Frisch, K. Raghavachari, and J. A. Pople, J. Phys. Chem. **86**, 1529 (1982).
[3] D. A. Dixon, A. Komornicki, and W. P. Kraemer, J. Chem. Phys. **81**, 3603 (1984).
[4] D. J. DeFrees and A. D. McLean, J. Comput. Phys. **7**, 321 (1986).
[5] N. L. Ma, B. J. Smith, J. A. Pople, and L. Radom, J. Am. Chem. Soc. **113**, 7903 (1991).
[6] N. L. Ma, B. J. Smith, and L. Radom, Chem. Phys. Lett. **197**, 573 (1992).
[7] Y. Yamaguchi, C. A. Richards, and H. F. Schaefer, J. Chem. Phys. **101**, 8945 (1995).
[8] P. W. Harland, N. D. Kim, and S. A. H. Petrie, Aust. J. Chem. **42**, 9 (1989).

[9] S. G. Lias, J. E. Bartmess, J. F. Liebman, J. L. Holmes, R. D. Levin, and W. G. Mallard, J. Phys. Chem. Ref. Data **17**, Suppl. 1 (1988).
[10] C. G. Freeman, J. S. Knight, J. G. Love, and M. J. McEwan, Int. J. Mass Spectrom. Ion Processes **80**, 255 (1987).
[11] A. Cunje, C. F. Rodriquez, D. K. Bohme, and A. C. Hopkinson, J. Phys. Chem. A **102**, 478 (1998).
[12] R. C. Woods, R. J. Saykally, T. G. Anderson, T. A. Dixon, and P. G. Szanto, J. Chem. Phys. **75**, 4256 (1981).
[13] C. S. Gudeman and R. C. Woods, Phys. Rev. Lett. **48**, 1344 (1982).
[14] W. Wagner-Redeker, P. R. Kemper, M. F. Jarrold, and M. T. Bowers, J. Chem. Phys. **83**, 1121 (1985).
[15] R. C. Woods *et al.*, Astrophys. J. **270**, 583 (1983).
[16] L. M. Ziurys and A. J. Apponi, Astrophys. J. **455**, L 73 (1995).
[17] D. Buhl and L. E. Snyder, Nature (London) **228**, 267 (1970).
[18] A. J. Chalk and L. Radom, J. Am. Chem. Soc. **119**, 7573 (1997).
[19] D. K. Bohme, Int. J. Mass Spectrom. Ion Processes **115**, 95 (1992).
[20] A. J. Chalk and L. Radom, J. Am. Chem. Soc. **121**, 1574 (1999).
[21] E. P. L. Hunter and S. G. Lias, J. Phys. Chem. Ref. Data **27**, 413 (1998).
[22] GAUSSIAN94, Revision A.1, M. J. Frisch, G. W. Trucks, H. B. Schlegel, P. M. W. Gill, B. G. Johnson, M. A. Robb, J. R. Cheeseman, T. A. Keith, G. A. Petersson, J. A. Montgomery, K. Raghavachari, M. A. Al-Laham, V. G. Zakrzewski, J. V. Ortiz, J. B. Foresman, J. Cioslowski, B. B. Stefanov, A. Nanayakkara, M. Challacombe, C. Y. Peng, P. Y. Ayala, W. Chen, M. W. Wong, J. L. Andres, E. S. Replogle, R. Gomperts, R. L. Martin, D. J. Fox, J. S. Binkley, D. J. DeFrees, J. Baker, J. P. Stewart, M. Head-Gordon, C. Gonzalez, and J. A. Pople, Gaussian, Inc., Pittsburgh, PA, 1995.
[23] GAUSSIAN98, Revision A.6, G. W. Frisch, G. W. Trucks, H. B. Schlegel, G. E. Scuseria, M. A. Robb, J. R. Cheeseman, V. G. Zakrzewski, J. A. Montgomery Jr., R. E. Stratmann, J. C. Burant, S. Dapprich, J. M. Millam, A. D. Daniels, K. N. Kudin, M. C. Strain, O. Farkas, J. Tomasi, V. Barone, M. Cossi, R. Cammi, B. Mennucci, C. Pomelli, C. Adamo, S. Clifford, J. Ochterski, G. A. Petersson, P. Y. Ayala, Q. Cui, K. Morokuma, D. K. Malick, A. D. Rabuck, K. Raghavachari, J. B. Foresman, J. Cioslowski, J. V. Ortiz, B. B. Stefanov, G. Liu, A. Liashenko, P. Piskorz, I. Komaromi, R. Gomperts, R. L. Martin, D. J. Fox, T. Keith, M. A. Al-Laham, C. Y. Peng, A. Nanayakkara, C. Gonzalez, M. Challacombe, P. M. W. Gill, B. Johnson, W. Chen, M. W. Wong, J. L. Andres, C. Gonzalez, M. Head-Gordon, E. S. Replogle, and J. A. Pople, Gaussian, Inc., Pittsburgh, PA, 1998.
[24] B. J. Smith and L. Radom, J. Am. Chem. Soc. **115**, 4885 (1993).
[25] M. J. Frisch, Æ. Frisch, and J. B. Foresman, GAUSSIAN 94 *User's Reference* (Gaussian Inc., Pittsburgh, 1995)
[26] W. R. Wadt and P. J. Hay, J. Chem. Phys. **82**, 284 (1985).
[27] J. Ischtwan and M. A. Collins, J. Chem. Phys. **100**, 8080 (1994).
[28] M. J. T. Jordan, K. C. Thompson, and M. A. Collins, J. Chem. Phys. **102**, 5647 (1995).
[29] M. J. T. Jordan, K. C. Thompson, and M. A. Collins, J. Chem. Phys. **103**, 9669 (1995).
[30] M. J. T. Jordan and M. A. Collins, J. Chem. Phys. **104**, 4600 (1996).
[31] K. C. Thompson and M. A. Collins, J. Chem. Soc., Faraday Trans. **93**, 871 (1997).
[32] R. P. A. Bettens and M. A. Collins, J. Chem. Phys. **111**, 816 (1999).
[33] R. Farwig, in *Algorithms For Approximation*, edited by J. C. Mason and M. G. Cox (Clarendon, Oxford, 1987), p. 194.
[34] P. Lancaster and K. Salkauskas, *Curve and Surface Fitting, An Introduction* (Academic, London, 1986), Chap. 10.
[35] K. C. Thompson, M. J. T. Jordan, and M. A. Collins, J. Chem. Phys. **108**, 8302 (1998).
[36] M. P. Allen and D. J. Tildesley, *Computer Simulations of Liquids* (Clarendon, Oxford, 1987), p. 146.
[37] H. W. Schranz, S. Nordholm, and G. Nyman, J. Chem. Phys. **94**, 1487 (1991).
[38] R. P. A. Bettens and M. A. Collins, J. Chem. Phys. **108**, 2424 (1998).
[39] R. P. A. Bettens and M. A. Collins, J. Chem. Phys. **109**, 9728 (1998).
[40] R. P. A. Bettens, T. Hansen, and M. A. Collins, J. Chem. Phys. **111**, 6322 (1999).
[41] M. A. Collins and D. H. Zhang, J. Chem. Phys. **111**, 9924 (1999).
[42] T. M. Miller, in *CRC Handbook of Chemistry and Physics* (CRC Press, Boca Raton, FL, 1997), pp. 10–201.
[43] J. I. Steinfeld, J. S. Francisco, and W. L. Hase, *Chemical Kinetics and Dynamics* (Prentice–Hall, Englewood Cliffs, NJ, 1989), p. 272.
[44] R. G. Gilbert and S. C. Smith, *Theory of Unimolecular and Recombination Reactions* (Blackwell Scientific, Oxford, 1990), Chap. 3.